Computers and Geotechnics 161 (2023) 105576

Contents lists available at ScienceDirect

Computers and Geotechnics

journal homepage: www.elsevier.com/locate/compgeo

Unlined Length Effect on the Tunnel Face Stability and Collapse Mechanisms in c-ϕ Soils: A Numerical Study with Advanced Mesh Adaptive Strategies

Xiangcou Zheng [a,c], Feng Yang [a], Jim Shiau [d], Fengwen Lai [b,*], Daniel Dias [e]

[a] School of Civil Engineering, Central South University, Changsha, Hunan 410075, China
[b] Faculty of Civil Engineering and Geosciences, Delft University of Technology, Delft 2628 CN Delft, the Netherlands
[c] School of Engineering, University of Durham, Durham DH1 3LE, UK
[d] School of Engineering, University of Southern Queensland, QLD 4350, Australia
[e] Laboratory 3SR, Grenoble INP, CNRS, Grenoble Alpes University, Grenoble 38000, France

ARTICLE INFO

Keywords:
Tunnel face stability
Collapse mechanism
Upper bound limit analysis
Mesh adaptive updating strategy
Flow rule

ABSTRACT

This paper presents a stability study on the collapse mechanisms of a plane-strain tunnel face in c-ϕ soils using the upper bound finite element method with rigid translatory moving elements (UBFELA-RTME) and nonlinear programming technique. Practical considerations are given to the unlined length influence behind the tunnel face. An advanced mesh adaptive updating strategy is adopted, aiming to improve the computational efficiency, the accuracy of upper-bound solutions, as well as the produced collapse mechanisms. The unlined length influence on the face stability and collapse mechanism of the tunnel face are determined with various combinations of tunnel depth ratios, soil friction angles, and dilatancy angles. Using the UBFELA-RTME with the Davis's approach and a mesh adapting strategy, the non-associated plasticity flow rule can be well approximated. The developed technique was validated against different numerical methods, and it is concluded that the tunnel face stability can be improved by increasing soil friction and dilatancy angles, and yet weakens as the unlined length increases where a mesh-liked collapse zone gradually appears on the tunnel vault top. It gradually evolves to a global collapse failure till the ground surface. The findings contribute to a better understanding of the ground surface failure under the unlined support length influence in tunnel construction.

1. Introduction

Soil stability study related to the collapse mechanisms of a tunnel face is a classical but still ongoing field of research. Various methods of investigation were adopted for this problem. Experimental tests, such as physical tests and centrifuge modeling (Atkinson and Potts, 1977; Schofield, 1980; Mair et al., 1993; Chen et al., 2013), were employed to study the ultimate surface pressure to sustain the tunnel face stability as well as to study the associated collapse mechanisms. Based on the limit equilibrium concept, Eisenstein and Samarasekara (1992) analyzed the stability of unsupported shallow tunnels in clay with finite element analysis, whilst Anagnostou and Kovári (1994) investigated the limit support pressure needed for maintaining the tunnel face stability. Jancsecz and Steiner (1994) also studied the stability of a shield tunnel face according to the equilibrium of sliding wedges.

Based on the works presented by Drucker et al. (1951, 1952) and Chen (1975), limit analysis proved to be an efficient method, and in the past decades, it has been widely applied to the problem of tunneling face stability of underground openings (see e.g., Davis et al., 1980; Leca and Dormieux, 1990; Mollon et al., 2010; Lee and Nam, 2001; Subrin and Wong, 2002; Lee et al., 2003; Fraldi and Guarracino, 2009; Huang and Song, 2013, Yang and Huang, 2013; Zhang et al., 2017, Zou et al., 2019, Li et al., 2021). Using upper and lower bounds finite element limit analyses (FELA) with linear programming, Sloan and Assadi (1994) studied the undrained stability of a heading under surcharge loading. Augarde et al. (2003) extended the linear programming to non-homogeneous soils based on improved solution algorithms using nonlinear programming. Shiau et al. (2004, 2006, 2021), and Lai et al. (2022a, 2022b) adopted the latest FELA to various geotechnical stability applications. The flow rule influence on a stability problem was

* Corresponding author.
E-mail addresses: F.Lai-1@tudelft.nl, laifengwen@163.com (F. Lai).

https://doi.org/10.1016/j.compgeo.2023.105576
Received 9 December 2022; Received in revised form 1 June 2023; Accepted 6 June 2023
Available online 17 June 2023

discussed by Lai et al. (2022b) using the displacement finite element analysis (FEA) and a so-called "Davis approach" (Davis, 1968). Yang et al. (2016) analyzed the tunnel face stability subjected to a surcharge loading using the upper bound finite element method with rigid translatory moving elements (UBFELA-RTME). It was shown to be a more efficient numerical strategy to identify the underlying collapse mechanisms (Yang et al., 2014). In addition, it should be pointed out that other numerical methods including traditional mesh-based method, meshfree method and hybrid mesh-meshfree method can also be applied for analyzing the stability of the tunnel face. However, as the main focus of this study is to determine the unlined length effect on the tunnel face stability and collapse mechanisms using the UBFELA-RTME with advanced mesh adaptive strategies, more details regarding other numerical methods especially for those meshfree/mesh-meshfree methods are omitted and they can be found in some previous studies (Nguyen et al., 2008, 2023; Zheng et al., 2021, 2022).

Most of previous studies focused on the assumption that either the excavated tunnel has an infinitely stiff lining or is subjected to a constant internal pressure. This is especially true for shield-driven tunnels. Nevertheless, in New Austrian Tunneling Method (NATM), no supporting pressure is applied on the tunnel face due to the open-face excavation. Besides, there are unlined sections at the tunnel face rear, as supporting structures are not easy to install close to the tunnel face due to the tunneling operations. This unlined section may lead to a reduction of tunnel face stability, and even to a collapse. Therefore, being on the safe side, it is reasonable to consider both unlined sections and no supporting tunnel face in a tunnel design.

Based on the above discussions, the main objective of this study is to investigate the unlined sections effect on the stability and collapse mechanisms of a tunnel face in c-ϕ soils. Using the UBFELA-RTME method, advanced mesh adaptive updating strategies are introduced to improve the computational efficiency, the accuracy of numerical solutions, and the refinement of collapse mechanisms. A series of nonlinear upper bound finite element analyses considering various values of dimensionless unlined lengths L/D, tunnel buried depths H/D, soil frictional angles ϕ, and dilatancy angles ψ are performed. The variations of the stability number N and of the tunnel face collapse mechanisms with L/D, H/D, ϕ, and ψ are also studied. Stability charts as well as the associated collapse mechanisms are presented for practical references.

2. Problem definition

Fig. 1(a) shows the problem definition, where an idealized plane-strain tunnel face stability model in c-ϕ soils with a tunnel height D and depth H is presented. The soil mass is assumed to be a uniform Mohr-Coulomb material, and has a unit weight γ, drained friction angle ϕ, and cohesion c, as well as a dilatancy angle ψ. The ground surface is horizontal with no surcharge loading, and the tunnel collapse is assumed to be only initiated by the soil self-weight action. At the tunnel roof, an unlined heading of length L is located between the rigid lining and the tunnel face. The unlined sections at the rear-bottom of tunnels have practically no influence on the tunnel face stability (Senent et al., 2020), they are therefore not considered in the present study.

A typical finite element model with mesh discretization and boundary conditions for the proposed upper bound problem is shown in Fig. 1(b). The extents of the domain are denoted as L_1, L_2, and L_3, and they are chosen to be sufficiently large to ensure no boundary effects on the obtained results. For the boundary conditions, $u = 0$ and $v = 0$ represent "fixed" condition in the x and y directions respectively. The domain is artificially discretized into a series of three-node rigid triangular elements with a gradually reduction of size towards the tunnel face. Each node remains unique to a particular element, and therefore, velocity discontinuities can be allowed along all interfaces between elements.

The tunnel face stability is studied using a dimensionless stability number N that is a function of L/D, ϕ, ψ, and H/D and is expressed using equation (1).

$$N = \gamma D/c = f(L/D, \phi, \psi, H/D) \tag{1}$$

With the given values of D and c, the N values can thus be calculated by substituting the obtained γ values from the analysis output (this will be further explained in the next section). In all analyses, L/D ranges from 0 to 0.6, ϕ from 0° to 35°, ψ from 0° to 35°, and H/D from 1 to 4. Notice that, in this study, the c-ϕ soils are considered to be homogeneous. In reality, though, it is particularly likely that there will be significant uncertainties in the soil properties. These uncertainties may have considerable effects on the obtained deterministic solutions, and their influences will be determined by incorporating different types of model uncertainties (Ding et al., 2019; Hauseux et al., 2017; Rappel et al., 2018, 2019, 2020) in a future study.

3. Mesh adaptive updating strategy and UBFELA-RTME

As stated in Yang et al. (2015a), rigorous solutions to the ultimate failure characteristics of geotechnical problems and their associated collapse mechanisms can be obtained by using mesh-liked rigid block systems in the UBFELA-RTME. In this method, a refined initial mesh is beneficial for obtaining more rigorous upper-bound solutions and the associated failure modes. Nevertheless, it would greatly increase the computational effort, making the solving process of nonlinear programming become quite difficult. This is particularly for soils with high

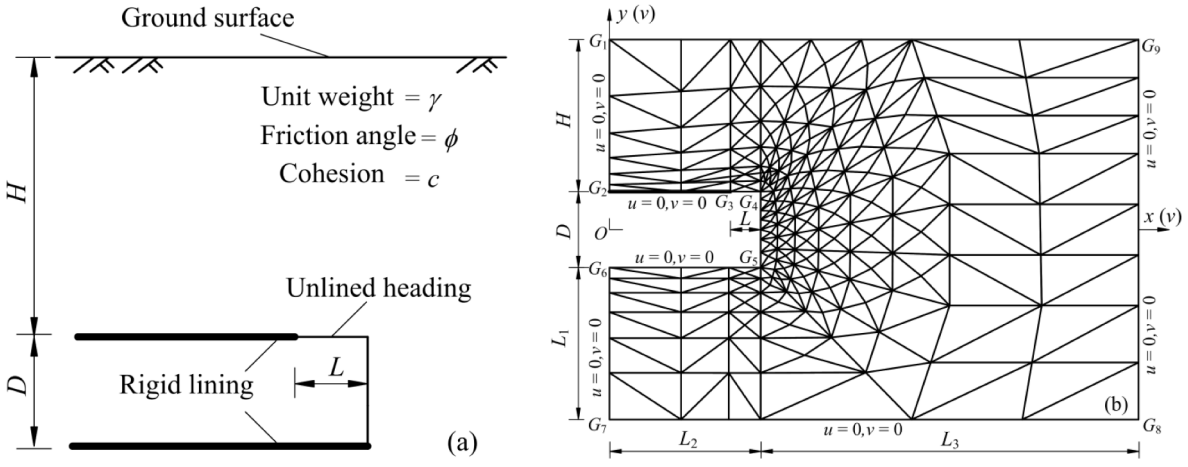

Fig. 1. Problem definition: (a) geometric layout and (b) mesh discretisation and boundary conditions.

friction angles, where the dilatancy effects cannot be ignored and the assumption of associated flow rule of the upper bound theorem becomes unrealistic to evaluate (Sloan, 2013). To overcome these difficulties and improve the accuracy of upper-bound solutions, a mesh adaptive updating strategy is proposed and implemented in MATLAB. The strategy consists of (1) elements merging and eliminating, (2) mesh refining, and (3) mesh inheritance and correction. More details are explained as follows.

Yang et al. (2015a) showed that only a small part of the velocity discontinuities is truly active during the optimization process. Thus, the mesh division for the UBFELA-RTME can be updated by selectively the merging adjacent elements with no-relative velocity and then eliminating those with zero areas. As an example, the major merging and eliminating process for the element *ACD* is shown in Fig. 2(a). Note that the adjacent element with an identical side *AD* is merged and eliminated. For mesh refining, it was found that the collapse mechanisms are mainly comprised of several groups of velocity discontinuities in the main collapse zone that resembles to slip lines. Therefore, mesh refining in major collapse areas may directly affect the accuracy of the upper bound solutions and the collapse mechanisms refinement. Fig. 2(b) presents a mesh refining strategy, combined with element merging and eliminating steps, with one mother element (I) discretizing into eight (II) or four (III or IV) child elements. For smaller soil friction angles, a suitable initial solution is always easier to obtain using UBFELA-RTME. Therefore, the final mesh division can be inherited as the initial mesh for soils with higher friction angles. The drawback due to the associated flow rule assumption can be also remediated to some extents using the proposed strategy, which will be discussed below. To achieve this, the mesh updating strategy and some small necessary corrections are required during the optimization process. It should be pointed out that different refinement criteria may have a nonneglectable impact on the final pattern of refined meshes. Therefore, there are alternatives to simple goal-oriented mesh adaptation strategies (González-Estrada et al., 2014, Bulle et al., 2023), which might be suitable for the UBFELA-RTME but are not studied. In addition, as mesh refinements in major collapse areas with high energy dissipation velocity discontinuities are performed in this study, which is slightly different from that in the traditional FEM with finite elements undergo plastic deformation.

Considering UBFELA-RTME, a nonlinear programming model for the tunnel face stability is formulated by minimizing the power dissipated along all velocity discontinuities minus the soil self-weight work. The objective function and constraints of this nonlinear optimization problem can therefore be presented as follows:

$$\gamma_{cr} = \sum_{i=1}^{n_d} P_{d,i} \tag{2}$$

where γ_{cr} is the critical unit weight of the soil mass that a tunnel face can withstand, and it is subjected to the following constraints (equations (3.1) to (3.12)).

$$-\xi_i^{'} - \xi_i^{''} \leqslant 0;\ \ \xi_i^{'} - \xi_i^{''} \leqslant 0;\ \ (i = 1, \ldots, n_d) \tag{3.1}$$

$$-A_i < 0; (i = 1, \ldots, n_t) \tag{3.2}$$

$$\sum_{i=1}^{n_t} A_i(-v_i) = 1 \tag{3.3}$$

$$G_1G_2 : u_i = 0, v_i = 0; x_j = 0, \frac{D}{2} \leq y_j \leq H + \frac{D}{2};\ \ (j = 1, \ldots, n_{g1}) \tag{3.4}$$

$$G_2G_3 : u_i = 0, v_i = 0; 0 \leq x_j = L_2 - L, y_j = \frac{D}{2}; \left(i = 1, \ldots, n_{v2}, j = 1, \ldots, n_{g2}\right) \tag{3.5}$$

$$G_3G_4 : u_i = 0, v_i = 0; L_2 - L \leq x_j \leq L_2, y_j = \frac{D}{2};\ \ (i = 1, \ldots, n_{v3}, j = 1, \ldots, n_{g3}) \tag{3.6}$$

$$G_4G_5 : x_j = L_2,\ -\frac{D}{2} \leq y_j \leq \frac{D}{2};\ \ (j = 1, \ldots, n_{g4}) \tag{3.7}$$

$$G_5G_6 : u_i = 0, v_i = 0; 0 \leq x_j \leq L_2, y_j = -\frac{D}{2};\ \ (i = 1, \ldots, n_{v5}, j = 1, \ldots, n_{g5}) \tag{3.8}$$

$$G_6G_7 : u_i = 0, v_i = 0; x_j = 0,\ -L_1 - \frac{D}{2} \leq y_j \leq -\frac{D}{2};\ \ (i = 1, \ldots, n_{v6}, j = 1, \ldots, n_{g6}) \tag{3.9}$$

$$G_7G_8 : u_i = 0, v_i = 0; 0 \leq x_j \leq L_2 + L_3, y_j = -L_1 - \frac{D}{2};\ \ (i = 1, \ldots, n_{v7}, j = 1, \ldots, n_{g7}) \tag{3.10}$$

$$G_8G_9 : u_i = 0, v_i = 0; x_j = L_2 + L_3, -L_1 - \frac{D}{2} \leq y_j \leq H + \frac{D}{2}; \left(i = 1, \ldots, n_{v8},\ j = 1, \ldots, n_{g8}\right) \tag{3.11}$$

$$G_1G_9 : 0 \leq x_j \leq L_2 + L_3, y_j = H + \frac{D}{2};\ \ (j = 1, \ldots, n_{g9}) \tag{3.12}$$

Eq. (3.1) ensures the associated flow rule along the velocity discontinuities and Eq. (3.2) makes sure that each element area remains positive. According to the upper bound theorem, Eq. (3.3) stipulates that the objective function is equal to the critical unit weight of soils. Eqs. (3.4) to (3.12) define the constraints along other boundaries, respectively. Note that all elements' velocities and nodal coordinates are treated as decision variables to be determined. More details of the formulation can be found in Yang et al. (2015a, 2015b).

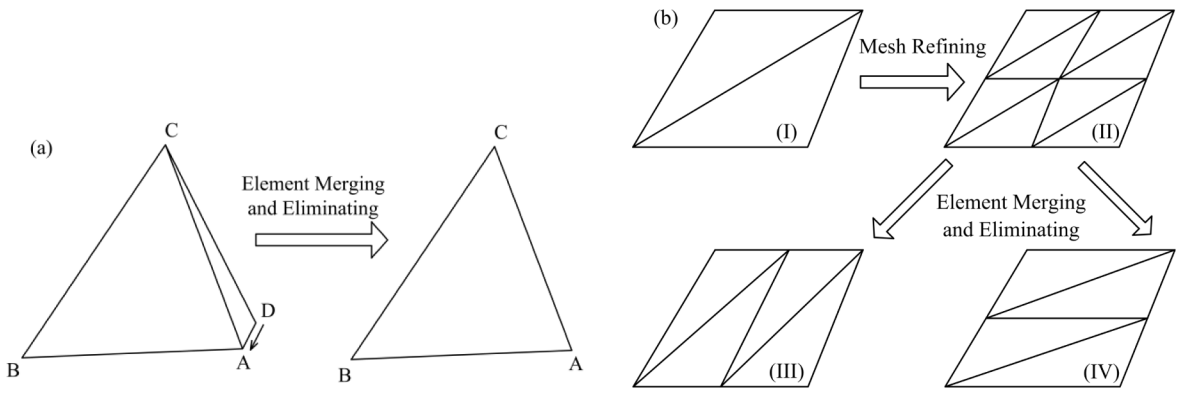

Fig. 2. Main principle of mesh adaptive updating: (a) element merging and eliminating; (b) mesh refining.

4. Consideration of flow rule

It is well known that the FELA is limited to soils with an associated plasticity ($\phi = \psi$), which is not realistic for soils in general. Tschuchnigg et al. (2015a, 2015b) and Schmudderich et al. (2022) demonstrated that the flow rule effect on some boundary value problems (e.g., stability of steep slopes, passive earth pressure problems) would be significant and cannot be neglected. As highlighted by Lai et al. (2022b), the drawback due to this assumption can be remediated to some extents by running FELA analyses where non-associated flow ($\phi < \psi$) is approximated with reduced strength parameters from Davis's approach(Davis, 1968) or by running displacement finite element analyses (FEA) where a non-associated plasticity can be considered. Using a reduction factor β, the Davis's approach to obtained reduced soil strength parameters can be written using Eq. (4).

$$c^* = \beta c \tag{4.1}$$

$$\phi^* = \beta tan\phi \tag{4.2}$$

$$\beta = \frac{cos\psi cos\phi}{1 - sin\psi sin\phi} \tag{4.3}$$

Indeed, the flow rule influence on the tunnel face stability problems in soil with high friction angles is still unclear yet requires further investigation. This will be determined in this paper using the Davis's approach.

5. Comparison and validation

5.1. Soil with low friction angle

To validate the effectiveness of the UBFELA-RTME with the mesh adaptive updating strategy in soils with low friction angles, Fig. 3 presents the mesh adaptive updating process for tunnel face with $L/D = 0.4$, $H/D = 2$, $\phi = 5°$, and $\psi/\phi = 1$. The initial structured mesh discretization gives similar results to the ones shown earlier in Fig. 1 (b), and the initial numbers of elements n_e, nodes n_n, and velocity discontinuities n_v are 391, 221, and 562, respectively. The deformed mesh is presented in Fig. 3(a), and the updated mesh is shown in Fig. 3(b) after substituting the optimized nodal coordinates into the initial mesh. The respective n_e, n_n, and n_v values reduce to 49, 33, and 66. Based on this updated mesh, the obtained N value is equal to 2.22, which is 0.45% lower than the initial value of 2.23. The proposed mesh significantly reduced the computational scale of the model, and substantially improved the upper bound solutions.

To further improve the solutions accuracy, the mesh refining strategy is repeatedly performed, and the final updated mesh is presented in Fig. 3(c). The corresponding N value is equal to 2.21 for Fig. 3(c), and it is 0.9% smaller than for the one presented in Fig. 3(a). It was found that by repeatedly performing the adaptive mesh refining process, it is possible to improve the solution accuracy and produce a more refined collapse mechanism. The main drawback is the increased CPU time during the nonlinear optimization due to the increase of the computational scale. This is similar to the traditional displacement finite element method, in which convergence study is required to determine the best possible mesh for a limited number of elements. In order to keep a good balance between the prescribed accuracy and computational time, it is suggested to have a rational number of repeated processes for the mesh refinement using the proposed mesh updating strategy. It should be noted that the greater significance of the mesh adaptive updating strategy lies on mesh inheritance and correction. This is especially important for soil with high friction angles. Computational experience suggested that an accurate solution cannot be directly obtained merely based on an initial mesh division. It is also concluded that the proposed upper bound solutions for high values of ϕ are more sensitive to the mesh divisions.

To validate the stability number in soil with low friction angle, the N values calculated based on $L/D = 0$ (i.e., an infinitely strong lining) are compared with those of Davis et al. (1980) and Sloan and Assadi (1994) with $\phi = 0°$ as well as with Yang et al. (2015) with ϕ ranging from 5° to 20°. The comparison is shown in Fig. 4. In general, these results are in good agreement. For $\phi = 0°$, the present results are based on the average between the upper and lower bound solutions of Sloan and Assadi (1994). They are slightly greater than those lower bound solutions of Davis et al. (1980). For $\phi > 0°$, the present results compare extremely well with the upper bound solutions of Yang et al. (2015a). The use of the proposed strategy in soils with higher friction angles will be discussed in the following parts.

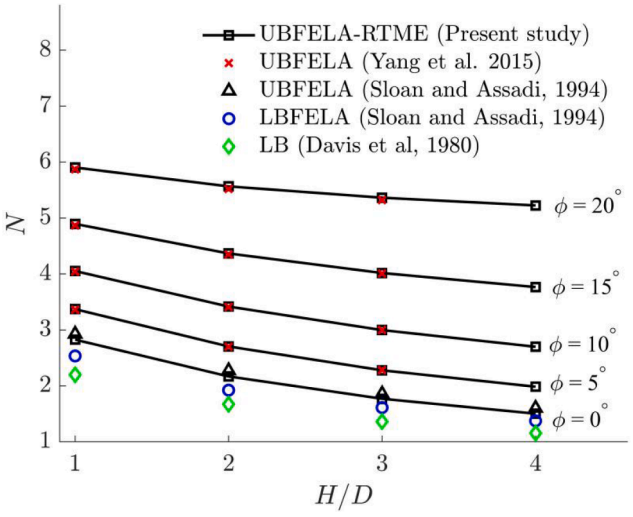

Fig. 4. Comparison of N between the proposed solutions and the previous solutions with $L/D = 0$, $H/D = 2$, $\phi = 5°$, and $\psi/\phi = 1$.

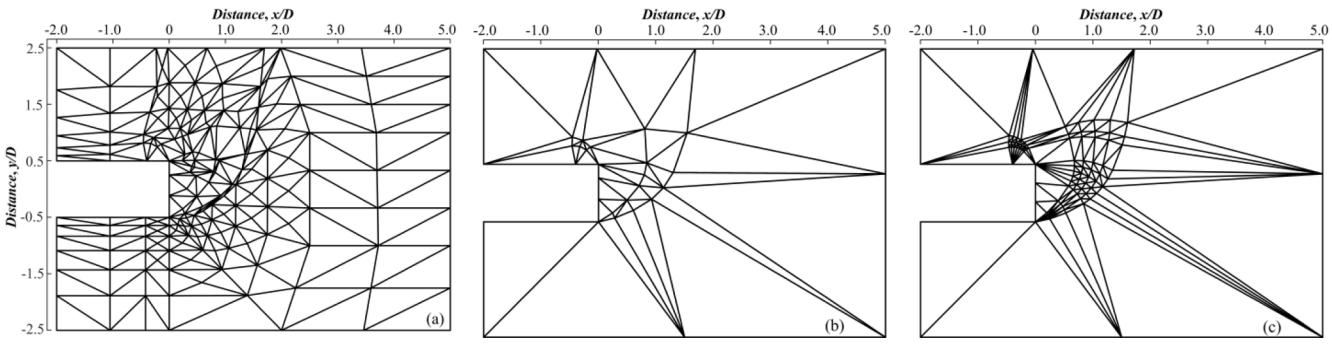

Fig. 3. Application of mesh adaptive updating in stability problem of the tunnel face.

5.2. Soil with high friction angle

The feasibility of the UBFELA-RTME with the mesh adaptive updating strategy in soils with high friction angle is examined through examples with $L/D = 0.4$, $H/D = 2$, $\phi = 35^\circ$ for $\psi = 0^\circ$ (non-associated) and $\psi = 35^\circ$ (associated). Table 1 presents a comparison of the stability number N obtained by the UBFELA-RTME, the UBFELA (Optum G2) (Krabbenhøft, 2019) and standard FEA (Plaxis 2D) (Brinkgreve et al., 2019) with different numbers of elements. It can be observed that the value of N from the UBFELA-RTME with 328 rigid triangle elements (associated) matches quite well with FEA-Plaxis 2D with 6682 elements (associated), and with UBFELA-Optum G2 with 3150 elements (associated). This confirms that the UBFELA-RTME can provide sufficiently accurate results with very few elements, which indicates a relatively high computational efficiency. Although adaptive mesh refinement technique is also involved in Optum G2, it still requires 8–10 times of the total number of elements to yield the almost same values of N as the UBFELA-RTME and the FEA.

Numerical results for the flow rule influence on the stability number are also presented in Table 1. The excellent agreement of the stability number N for non-associated materials between the UBFELA-RTME with the Davis approach and standard FEA can be observed. The UBFELA-RTME with the Davis approach (2500 elements) agree well with the Optum G2 with the Davis approach (2500 elements) and the FEA-Plaxis 2D (6682 elements). Therefore, it can be concluded that using the UBFELA-RTME with the Davis approach can well reproduce the flow rule influence on the tunnel face stability with an unlined length in high friction angle soils.

The comparison of tunnel face collapse mechanisms in associated materials ($\phi = \psi = 35^\circ$) obtained from three numerical methods are presented in Fig. 5. The FEA result is shown using total displacement contours, while FELA results are shown with final adaptive meshes. From Fig. 5, it can be found that the UBFELA-RTME provides a clear collapse mechanism (conical shape), which matches quite well with the FEA result. For Optum G2, although shear bands can be observed through a mesh refinement, the whole collapse zone is not clearly identified. Therefore, the merits of the UBFELA-RTME are on the one hand to provide accurate numerical solutions, e.g., the stability number and collapse mechanism for a stability problem, and on the other hand to well approximate a non-associate flow rule combining with the Davis approach. In the following work, the dilatancy angle influence on the stability and collapse mechanisms is also discussed using the UBFELA-RTME with the Davis approach.

5.3. Mesh convergence study

To further demonstrate the suitability of the proposed mesh adaptive scheme, Fig. 6(a) gives the relationship between the obtained stability number N and the total number of elements for the tunnel face with $H/D = 2$ and $\phi = 10^\circ$. It can be seen that more rigorous upper bound solution are gradually obtained when the total number of elements increases. This convergent solution confirms the computational performance of the proposed adaptive scheme. More quantitatively, Fig. 6(b) displays the relative error e_p of the obtained values of N upon mesh refinement, which is defined as follows:

$$e_p = \frac{N - N^*}{N^*} \tag{5}$$

where N^* is the reference stability number, and it is defined as the average value between the upper and lower bound solutions calculated using Optum G2 (with a total number of 10,000 elements). A gradual reduction in the value of e_p upon adaptive mesh refinement is observed, with a convergence rate varying between 1 and 2 as the major collapse domain is more finely discretised. This finding confirms the feasibility of integrating the proposed mesh adaptive schemes with the UBFELA-RTME.

Table 1
Comparison of stability number N from different numerical methods.

Numerical method	Element number	Flow rule	N
UBFELA-Optum G2	328	Assoc.	8.526
(Adaptive)	3150	Assoc.	7.374
	Assoc.-Davis	Assoc.-Davis	4.888
	Assoc.		6.144
UBFELA-RTME	328		7.371
(Adaptive)	337	Assoc.-Davis	6.148
FEM-Plaxis 2D	6682	Assoc.	7.342
	6682	Non-assoc.	6.147

6. Parametric studies and design charts

The effects of unlined lengths L/D on the tunnel face stability number N are presented in Fig. 7 for different values of H/D with $\phi = 15^\circ$ (Fig. 7 (a)) and $\phi = 35^\circ$ (Fig. 7(b)). The N values decrease almost linearly for soils with lower friction angles ($\phi = 15^\circ$) and non-linearly for soils with higher friction angles ($\phi = 35^\circ$) as L/D increases. The presence of unlined sections weakens the tunnel face stability, and therefore N decreases as L/D increases. The decrease rate is more pronounced for soil with large value of ϕ (as shown in Fig. 7(b)). In addition, for small values of ϕ (Fig. 6(a)), the greater the H/D, the lower the N. Interestingly, as shown in Fig. 7(b), for large values of $\phi = 35^\circ$, the parameter H/D has a negligible effect on the stability number N. It can be well explained by the strong soil arching effect due to the high frictional materials (Shiau and Al-Asadi, 2018, 2021). The depth influence on the tunnel face stability N would become very slight as the soil arching effect increases in particularly for high friction angles (e.g., $\phi = 35^\circ$). This would be further explained using the corresponding failure mechanisms in a later section.

The dilatancy angle (flow rule) influence on the stability number N is also explored in Fig. 7. Note that $\psi/\phi = 1$ represents that soil obeys the associated flow rule, and $\psi/\phi < 1$ represents a soil which obeys a non-associated flow rule. As expected, the N value increases with increasing the dilatancy angle. This effect would be more pronounced for higher friction angles. One can find that the difference of N between $\psi/\phi = 0$ and $\psi/\phi = 1$ for $\phi = 35^\circ$ is larger than for $\phi = 15^\circ$. It illustrates that the dilatancy angle (flow rule) effect on the stability number is required to be considered in the design of tunnelling, in particularly for strong frictional materials. The Davis approach has been confirmed as an alternative way to approximate the dilatancy angle effect on the stability number. Therefore, practical design charts can be given in materials following associated flow rule ($\psi/\phi = 1$) and with reduced strength parameters from the Davis approach.

To quantify the L/D effect on the tunnel face stability, an influence coefficient K_r is introduced. It is defined by ratios of the N values with non-zero L/D to those with $L/D = 0$. Fig. 8 shows the variations of K_r with L/D under different values of ϕ (0° to 20°) and H/D. The results indicate that the K_r values decrease approximate linearly with L/D. For all considered cases, the reduction in K_r can be up to 40%. The tunnel face stability is significantly affected by the unlined sections.

Fig. 9 shows the variation of stability number N against ϕ for different considered values of L/D and H/D. For such comprehensive design charts, in general, the values of N increase nonlinearly with an increase in ϕ, and this increased tendency becomes apparent for $\phi \geq 15^\circ$. This trend can be explained by the soil arching effect with greater values of ϕ. With the arching effect existence, the soil mass can resist a greater loading and therefore the tunnel face is more stable. In addition, for all considered tunnel geometries and soil conditions, the values of N are found to vary between 1.23 and 9.28. Note that a specific dilatancy angle can be specified to calculate the newly replaced values of c^* and ϕ^* using equations (4.1) to (4.3), so as to study the effect of non-associated flow rule.

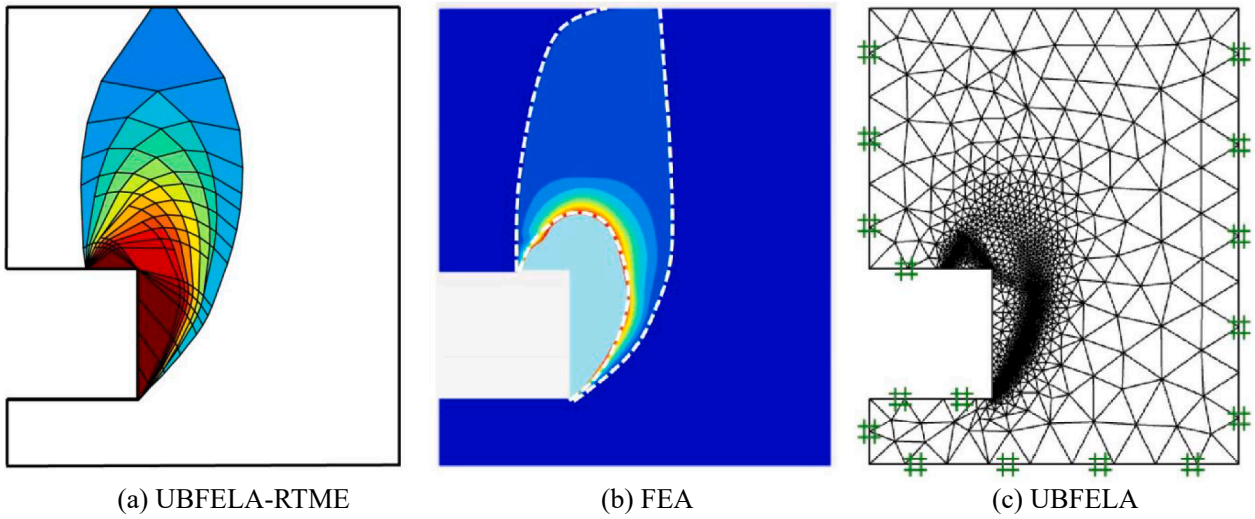

Fig. 5. Comparison of collapse mechanism obtained from UBFELA-RTME, FEA and UBFELA with $L/D = 0.4$, $H/D = 2$, $\phi = 35°$, and $\psi/\phi = 1$.

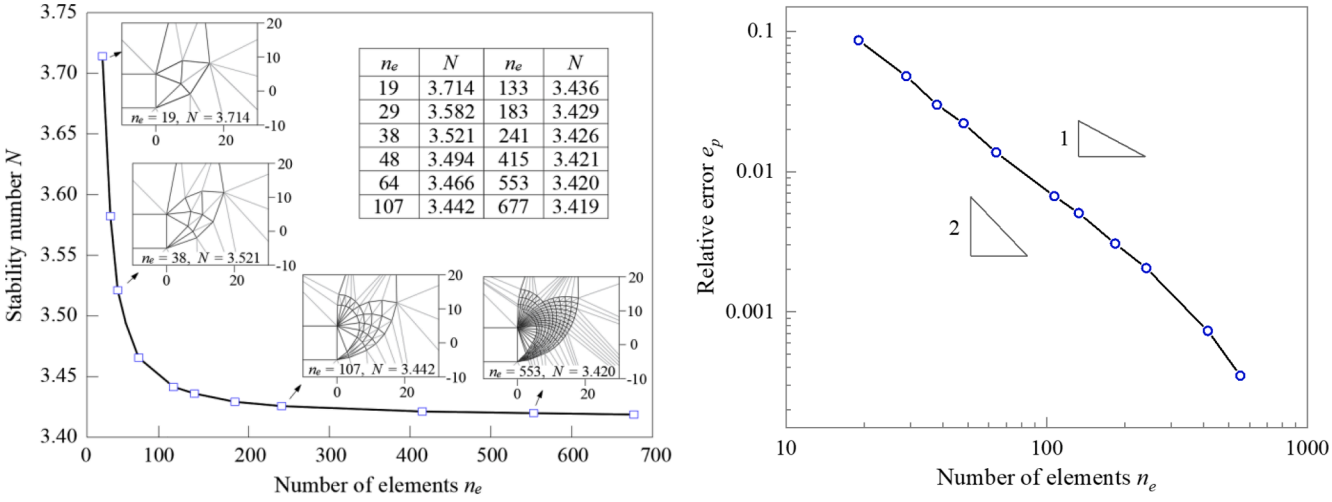

n_e	N	n_e	N
19	3.714	133	3.436
29	3.582	183	3.429
38	3.521	241	3.426
48	3.494	415	3.421
64	3.466	553	3.420
107	3.442	677	3.419

Fig. 6. Evolution of stability number N and relative error e_p with an increased number of elements n_e for the tunnel face with $H/D = 2$ and $\phi = 10°$.

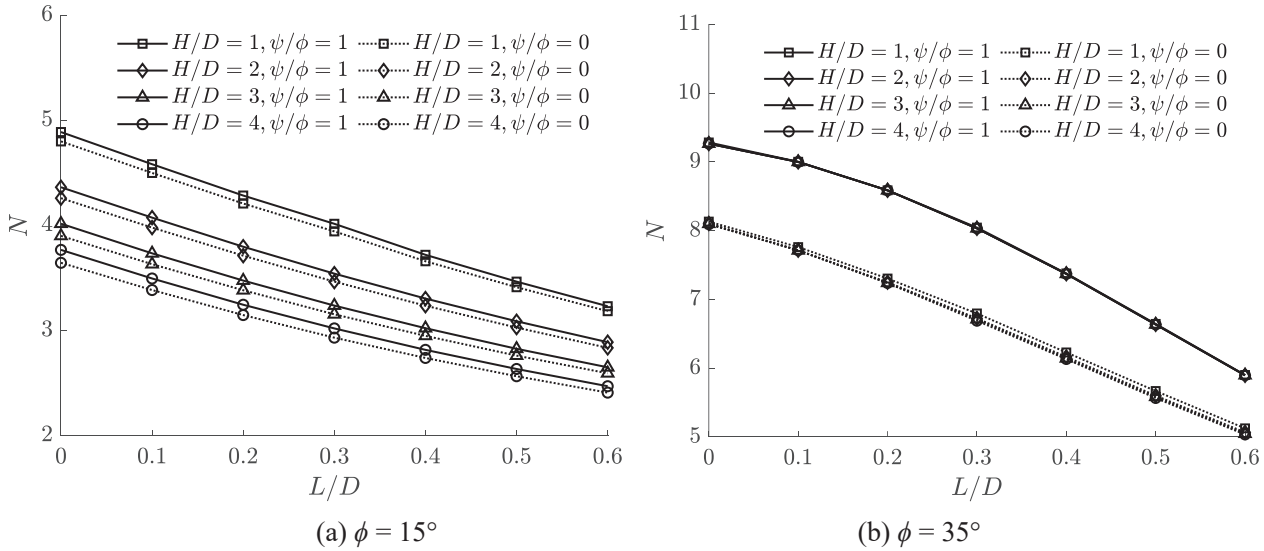

Fig. 7. Variations of N with L/D for various H/D under $\phi = 15°$ and $\phi = 35°$ ($\psi/\phi = 0$ and 1).

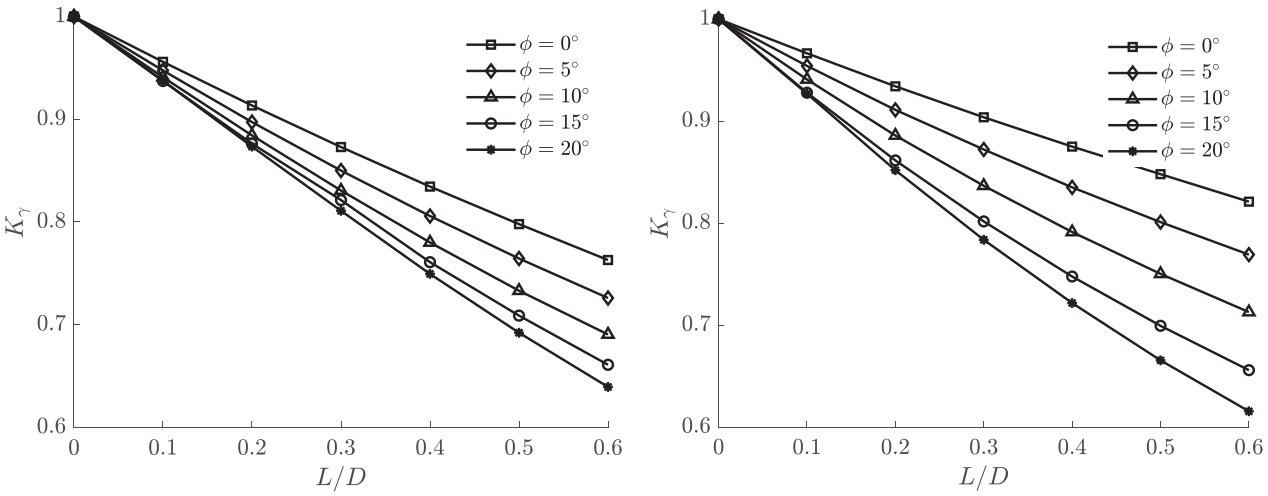

(a) $H/D = 1$ (b) $H/D = 4$

Fig. 8. Variations of K_γ with L/D for various ϕ under (a) $H/D = 1$; (b) $H/D = 4$.

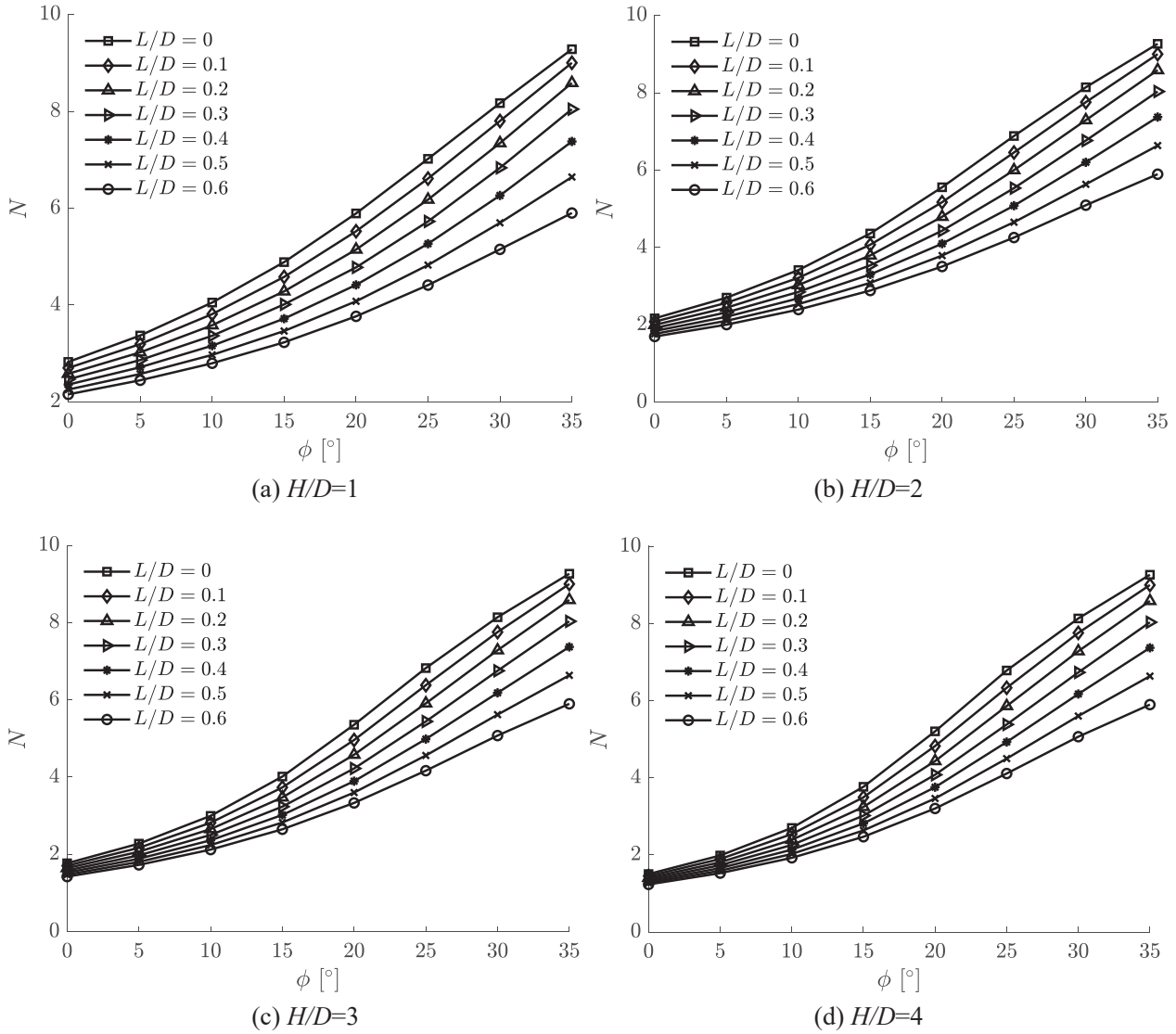

(a) H/D=1 (b) H/D=2

(c) H/D=3 (d) H/D=4

Fig. 9. Variations of N with ϕ for various L/D under (a) $H/D = 1$; (b) $H/D = 2$; (c) $H/D = 3$; (d) $H/D = 4$.

7. Collapse mechanisms

The tunnel face collapse mechanisms with the unlined sections presence are discussed in this section. Using the UBFELA-RTME, the collapse mechanisms are shown with "active" velocity discontinuities and model boundaries. The presented mechanisms are based on a series of mesh adaptive updates with deletions of the non-active ones. As shown in Fig. 10, the tunnel face collapse mechanisms consist of two groups of active velocity discontinuities (black lines) and two completely rigid blocks at the unlined section top and in the major collapse zone respectively. For a better interpretation, the absolute velocities are superimposed, where the red regions indicate elements with greater velocities and the light blue regions indicate elements with small velocities. In the following, the effects of L/D, H/D, and ϕ on the variations of collapse mechanisms are discussed.

7.1. Effect of unlined length L/D

As shown in Fig. 10(a), the conical tunnel face collapse mechanism primarily consists of a mesh-liked translational and rotational movements of soils in front of the tunnel face. Note that the collapse zone gradually extends to the ground surface to form a global failure mechanism. In addition, elements with the maximum absolute velocities are only located in local areas just in front of the tunnel face. They can be identified by the shear bands, and indeed, these collapse mechanisms are similar to the rigid block mechanisms proposed by Leca and Dormieux (1990) and Mollon et al. (2010).

On the other hand, with the unlined section ($L/D > 0$), the collapse patterns (Fig. 10(b)-10(d)) are mainly comprised by two mesh-liked collapse areas, locating on the top of the unlined section and at the front of the tunnel face. As L/D increases, the stability number N decreases, and the area of collapse zone increases. It can therefore be concluded that the presence of a local collapse area on the tunnel top vault would directly weaken the tunnel face stability and significantly reduce the bearing loading that can be resisted by the soil mass. The collapse zone on the unlined section top would play a dominant role in the whole collapse mechanisms as $L/D > 0$. Noting that elements with the maximum absolute velocities are densely distributed near the local area on the unlined section top and at the tunnel face front, the collapse mechanisms are greatly changed and are quite different from those with zero unlined length (Fig. 10(a)). Moreover, as the unlined section length increases, the lining constraint on the soil mass tends to reduce, and this leads to a decrease in the values of absolute velocities. It is recommended that more attention has to be given to the tunnel vault collapse on top of unlined sections during tunnel construction.

7.2. Effect of soil friction angle ϕ

The values of ϕ also have a pronounced influence on both the scopes and forms of the collapse mechanism. Fig. 11 shows the changes in collapse mechanisms with various values of ϕ for the case of $L/D = 0.3$ and $H/D = 2$. The collapse mechanisms showed that, with an increase in ϕ, the overall collapse zone decreases and the stability number N increases. It is interesting to observe the relative movements between blocks. The velocity discrepancy (i.e., the differences of regional color) becomes more intensive for soils with high values of ϕ. This finding also explains the difficulty in obtaining effective initial solutions for high values of ϕ as well as the associated collapse mechanisms.

7.3. Effect of tunnel buried depth H/D

To study the influence of the tunnel buried depth H/D on the tunnel face collapse mechanisms, cases for $L/D = 0.4$ and H/D varying from 1 to 4 are selected and they are shown in Figs. 11 and 12 respectively for $\phi = 20^\circ$ and 35°. For soils with small values of $\phi = 20^\circ$ in Fig. 12, the major tunnel face collapse mechanisms and absolute velocities of elements are proportionally similar to each other in spite of the H/D changes. The collapse zone increases dramatically and gradually extends deeper with an increase in H/D. For the considered buried depth ratios $H/D = 1$ to 4, the collapse zones extend to the ground surface (global failure). It would result in an active subsidence of the ground surface on the top and before the tunnel face. The widths of the active ground subsidence zone along tunnel excavation direction are found to increase from $0.83D$ to $1.34D$ with H/D varying from 1 to 4. The resulting stability numbers also decrease from 4.42 to 3.76 as H/D increases.

For $\phi = 35^\circ$, Fig. 13 shows the variations of the collapse mechanisms with H/D varying from 1 to 4. In the shallow case such as those shown in Fig. 13(a) and 13(b), the major collapse zones extend to the ground surface, in spite that the width of the active ground subsidence zone is smaller when it is compared with in the one in Fig. 12 ($\phi = 20^\circ$). Nevertheless, with a further increase in H/D, as shown in Fig. 13(c) and 13(d) for $H/D = 3$ and 4, a local failure pattern is found and the slip surface does not extend to the ground surface, which is a typical collapse form for deep tunnels. The major tunnel face collapse zones remain nearly unchanged. It is interesting to see that very small changes in the stability numbers as H/D increases. These observations compare well with those reported in Yang et al. (2017).

7.4. Effect of dilatancy angle ratio ψ/ϕ

The parametric studies have shown that the dilatancy angle ψ/ϕ effect on the stability number is more pronounced for a higher friction angle. To examine the dilatancy angle effect on the collapse

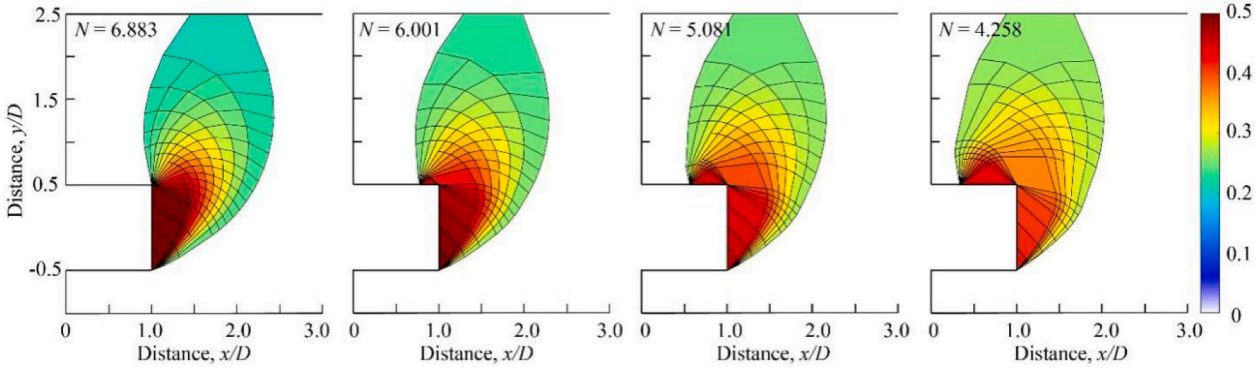

(a) $L/D = 0$ (b) $L/D = 0.2$ (c) $L/D = 0.4$ (d) $L/D = 0.6$

Fig. 10. Effect of unlined length L/D on collapse mechanism of tunnel face with $H/D = 2$, $\phi = 25^\circ$, and $\psi/\phi = 1$.

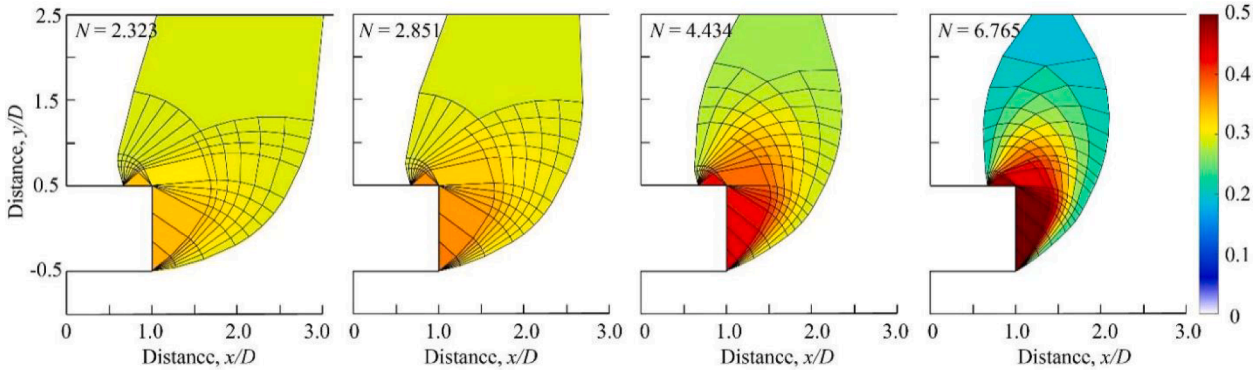

Fig. 11. Collapse mechanisms for various ϕ with $L/D = 0.3$, $H/D = 2$, and $\psi/\phi = 1$.

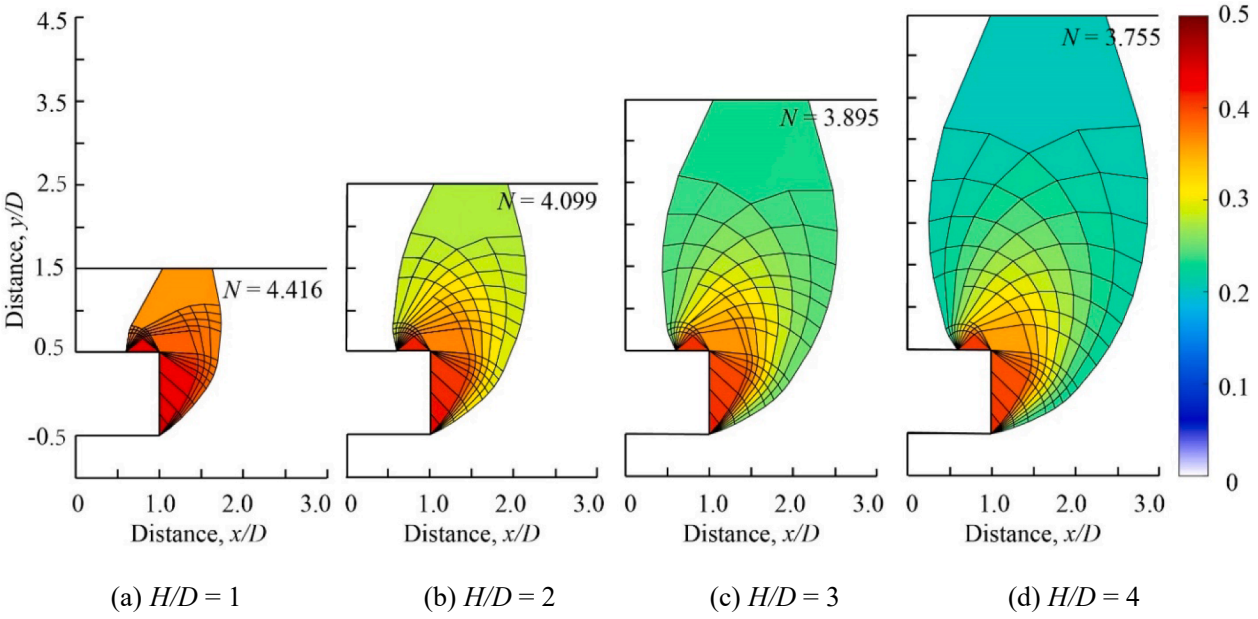

Fig. 12. Collapse mechanisms for various H/D with $L/D = 0.4$, $\phi = 20°$, and $\psi/\phi = 1$.

mechanisms, a comprehensive comparison between $\psi/\phi = 0$ and $\psi/\phi = 1$ for $\phi = 35°$ under various tunnel buried depths H/D is given in Fig. 13 and Fig. 14. For shallow buried tunnels (e.g., $H/D = 1$ and 2), although similar collapse mechanisms can be observed, there is a significant difference in the width of the active ground subsidence zone along the tunnel excavation direction between $\psi/\phi = 0$ and $\psi/\phi = 1$. A larger width for $\psi/\phi = 0$ is obtained, indicating weaker performance on tunnel face stability. It is of great interest that, for deep buried tunnels (e.g., $H/D = 3$ and 4), quite significant differences in collapse mechanism are observed, being one extending to ground surface (non-associate; Davis's approach), yet the other (associate) not.

In summary, the presented collapsed mechanisms in Fig. 10 demonstrates that unsupported tunnel face would compromise the tunnel stability, a larger unlined length enlarges the collapse zone. The presented tunnel face collapse mechanisms in Figs. 11-14 would suggest that the influence of H/D on the collapse mechanisms can be greatly affected by the values of ϕ and ψ. For soils with higher values of ϕ and ψ, the localized collapse arch on the tunnel vault top is more likely to form, as the soil arching effect enables the tunnel face to withstand larger loading and the tunnel heading becomes more stable.

8. Conclusions

This study investigated the stability and collapse mechanism of tunnel faces in c-ϕ soils under the influence of unlined lengths L/D. Using the UBFELA-RTME with the proposed mesh adaptive updating strategy, both the accuracy of stability numbers and the associated collapse mechanisms have been significantly improved. The variations of the stability number N, the influence coefficient K_r, and the associated collapse mechanisms for various values of L/D, H/D, ϕ and ψ were also discussed. The following conclusions can be drawn based on the current study.

(1) The values of N and K_r decrease almost linearly with L/D and H/D, but increase with ϕ and ψ. The presence of unlined sections tends to decrease the tunnel face stability up to a maximum of 40%.
(2) With the presence of unlined sections, a locally mesh-liked collapse area gradually emerges on the top of this unlined section, which directly weakens the tunnel face stability, and it would further dominate the whole collapse mechanism with a further increasing L/D.

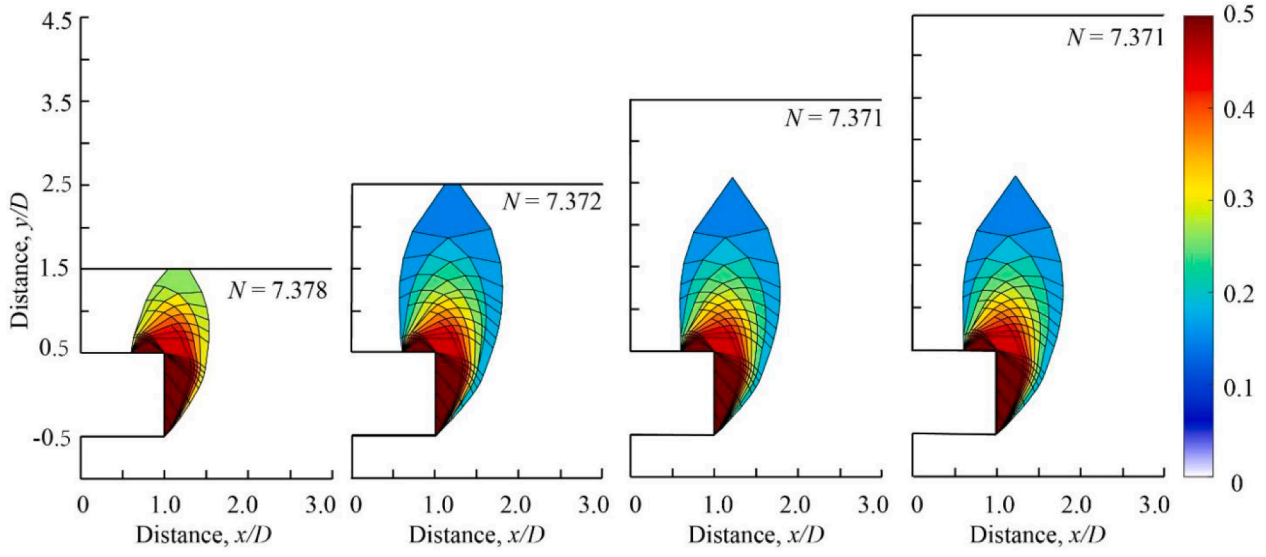

Fig. 13. Collapse mechanisms for various H/D with $L/D = 0.4$, $\phi = 35°$, and $\psi/\phi = 1$.

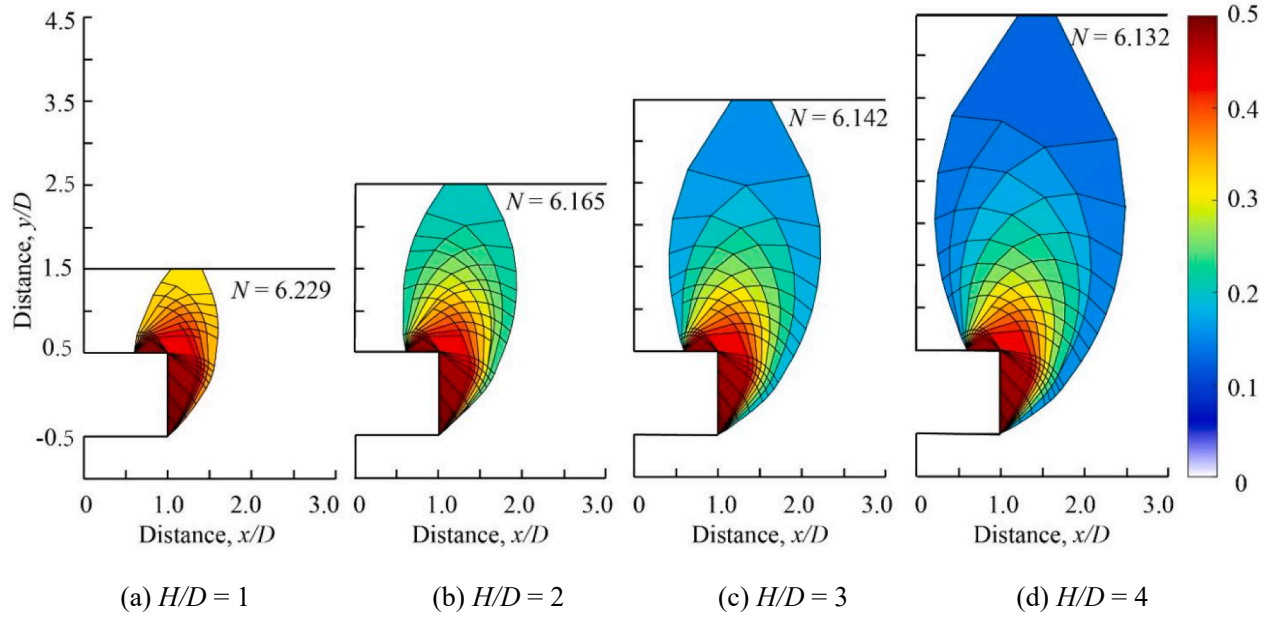

Fig. 14. Collapse mechanisms for various H/D with $L/D = 0.4$, $\phi = 35°$, and $\psi/\phi = 0$.

(3) The influence of H/D on the stability and collapse patterns of tunnel face is largely related to the values of ϕ. In some specific cases ($\phi > 30°$), the collapse zones of tunnel faces remain nearly unchanged as H/D increases. Owing to the soil arching effect, the failure zone does not extend to the ground surface, resulting in a local failure mechanism.
(4) The use of the UBFELA-RTME with the "Davis approach" and the proposed mesh adaptive updating strategy is a satisfactory alternative to approximate the non-associated plasticity. For high frictional materials, the dilatancy angle would significantly influence both the collapse mechanism and the stability number.

This research provides an improved understanding of both the stability and collapse mechanism of the tunnel face with the unlined sections influence. The current study paves the way for future researches with 3D analyses on the stability effects of unlined length of square and rectangular tunnels, as well as their associated collapse mechanisms. In addition, it is particularly interesting to address the impact of soil property uncertainties by incorporating advanced uncertainty models in a future study.

CRediT authorship contribution statement

Xiangcou Zheng: Methodology, Software, Validation, Formal analysis, Visualization, Writing – original draft, Writing – review & editing. **Feng Yang:** Conceptualization, Methodology, Funding acquisition, Writing – review & editing. **Jim Shiau:** Methodology, Writing – review & editing. **Fengwen Lai:** Methodology, Writing - review & editing. **Daniel Dias:** Methodology, Writing – review & editing.

Declaration of Competing Interest

The authors declare that they have no known competing financial interests or personal relationships that could have appeared to influence the work reported in this paper.

Data availability

Data will be made available on request.

References

Anagnostou, G., Kovári, K., 1994. The face stability of slurry shield-driven tunnels. Tunn. Undergr. Space Technol. 9 (2), 165–174.

Atkinson, J.H., Potts, D.M., 1977. Stability of a shallow circular tunnel in cohesionless soil. Géotechnique 27 (2), 203–215.

Augarde, C.E., Lyamin, A.V., Sloan, S.W., 2003. Stability of undrained plane strain heading revisited. Comput. Geotech. 30 (5), 419–430.

Brinkgreve, R.B.J., Kumarswamy, S., Swolfs, W.M., Zampich, L., Manoj, N.R., 2019. Plaxis 2D Material Models Manual. Delft, The Netherlands, Plaxis bv.

Bulle, R., Hale, J.S., Lozinski, A., Bordas, S.P., Chouly, F., 2023. Hierarchical a posteriori error estimation of Bank-Weiser type in the FEniCS Project. Comput. Math. with Appl. 131, 103–123.

Chen, W.F., 1975. Limit analysis and soil plasticity. Elsevier Science, New York.

Chen, R.P., Li, J., Kong, L.G., Tang, L.J., 2013. Experimental study on face instability of shield tunnel in sand. Tunn. Undergr. Space Technol. 33, 12–21.

Davis, E.H., 1968. Theories of plasticity and failures of soil masses. In: Lee, I.K. (Ed.), Soil mechanics: selected topics. Elsevier, New York, USA, pp. 341–354.

Davis, E.H., Guun, M.J., Mair, R.J., Seneviratne, H.N., 1980. The stability of shallow tunnels and underground openings in cohesive material. Géotechnique 30 (4), 397–416.

Ding, C., Deokar, R.R., Ding, Y., Li, G., Cui, X., Tamma, K.K., Bordas, S.P., 2019. Model order reduction accelerated Monte Carlo stochastic isogeometric method for the analysis of structures with high-dimensional and independent material uncertainties. Comput. Methods Appl. Mech. Eng. 349, 266–284.

Drucker, D.C., Greenberg, H.J., Prager, W., 1951. The safety factor of an elastic plastic body in plane strain. J. Appl. Mech. 18 (4), 371–378.

Drucker, D.C., Prager, W., Greenberg, H.J., 1952. Extended limit design theorems for continuous media. Q. Appl. Math. 9 (4), 381–389.

Eisenstein, Z., Samarasekara, L., 1992. Stability of unsupported tunnels in clay. Can. Geotech. J. 29 (4), 609–613.

Fraldi, M., Guarracino, F., 2009. Limit analysis of collapse mechanisms in cavities and tunnels according to the Hoek-Brown failure criterion. Int. J. Rock Mech. Min. Sci. 46 (4), 665–673.

González-Estrada, O.A., Nadal, E., Ródenas, J.J., Kerfriden, P., Bordas, S.P.A., Fuenmayor, F.J., 2014. Mesh adaptivity driven by goal-oriented locally equilibrated superconvergent patch recovery. Comput. Mech. 53 (5), 957–976.

Hauseux, P., Hale, J.S., Bordas, S.P., 2017. Accelerating Monte Carlo estimation with derivatives of high-level finite element models. Comput. Methods Appl. Mech. Eng. 318, 917–936.

Huang, M.S., Song, C.X., 2013. Upper-bound stability analysis of a plane strain heading in non-homogeneous clay. Tunn. Undergr. Space Technol. 38 (9), 213–223.

Jancsecz, S., Steiner, W., 1994. Face support for a large mix-shield in heterogeneous ground conditions. In: Tunnelling. Springer, US, pp. 531–550.

Krabbenhøft, K., Optum G2, 2019. Theory. Optum Computational Engineering.

Lai, F., Yang, D., Liu, S., Zhang, H., Cheng, Y., 2022a. Towards an improved analytical framework to estimate active earth pressure in narrow c–ϕ soils behind rotating walls about the base. Comput. Geotech. 141, 104544.

Lai, F.W., Zhang, N.N., Liu, S.Y., Yang, D.Y., 2022b. A generalised analytical framework for active earth pressure on retaining walls with narrow soil. Géotechnique 1–16.

Leca, E., Dormieux, L., 1990. Upper and lower bound solutions for the face stability of shallow circular tunnels in frictional material. Géotechnique 40 (4), 581–606.

Lee, I.M., Nam, S.W., 2001. The study of seepage forces acting on the tunnel lining and tunnel face in shallow tunnels. Tunn. Undergr. Space Technol. 16 (1), 31–40.

Lee, I.M., Nam, S.W., Jae, H.A., 2003. Effect of seepage force on tunnel face stability. Can. Geotech. J. 40 (2), 342–350.

Li, T., Gong, W., Tang, H., 2021. Three-dimensional stochastic geological modeling for probabilistic stability analysis of a circular tunnel face. Tunn. Undergr. Space Technol. 118, 104190.

Mair, R.J., Taylor, R.N., Bracegirdle, A., 1993. Subsurface settlement profiles above tunnels in clays. Géotechnique 43 (2), 315–320.

Mollon, G., Dias, D., Soubra, A.H., 2010. Face stability analysis of circular tunnels driven by a pressurized shield. J. Geotech. Geoenviron. 136 (1), 215–229.

Nguyen, V.P., Rabczuk, T., Bordas, S., Duflot, M., 2008. Meshless methods: A review and computer implementation aspects. Math. Comput. Simul. 79 (3), 763–813.

Nguyen, V.P., de Vaucorbeil, A., Bordas, S., 2023. The Material Point Method: Theory. Implementations and Applications, Springer Nature.

Rappel, H., Beex, L.A.A., Bordas, S.P.A., 2018. Bayesian inference to identify parameters in viscoelasticity. Mech. Time Depend. Mater. 22 (2), 221–258.

Rappel, H., Beex, L.A.A., Noels, L., Bordas, S.P.A., 2019. Identifying elastoplastic parameters with Bayes' theorem considering output error, input error and model uncertainty. Probabilistic Eng. Mech. 55, 28–41.

Rappel, H., Beex, L.A.A., Hale, J.S., Noels, L., Bordas, S.P.A., 2020. A tutorial on Bayesian inference to identify material parameters in solid mechanics. Arch. Comput. Methods Eng. 27 (2), 361–385.

Schmudderich, C., Tschuchnigg, F., Schweiger, H.F., 2022. Significance of flow rule for the passive earth pressure problem. Acta Geotech. 17 (1), 81–92.

Schofield, A.N., 1980. Cambridge Geotechnical Centrifuge Operations. Cambridge geotechnical centrifuge operations. Géotechnique 30 (3), 227–268.

Senent, S., Yi, C., Jimenez, R., 2020. An upper bound solution for tunnel face stability analysis considering the free span. Tunn. Undergr. Space Technol. 103, 103515.

Shiau, J.S., Al-Asadi, F., 2018. Revisiting Broms and Bennermarks' original stability number for tunnel headings. Géotech. Lett. 8 (4), 310–315.

Shiau, J.S., Al-Asadi, F., 2021. Revisiting circular tunnel stability using broms and bennermarks' original stability number. Int. J. Geomech. 21 (5), 06021009.

Shiau, J., Chudal, B., Mahalingasivam, K., Keawsawasvong, S., 2021. Pipeline burst-related ground stability in blowout condition. Transp. Geotech. 29, 100587.

Shiau, J.S., Lyamin, A.V., Sloan, S.W., 2004. Rigorous solution of classical lateral earth pressures. 6th Young Geotechnical Professionals Conference, Gold Coast, Australia. 162-167.

Shiau, J.S., Lyamin, A.V., Sloan, S.W., 2006. Application of pseudo-static limit analysis in geotechnical earthquake design. In: 6th European Conference on Numerical Methods in Geotechnical Engineering, 6-8 Sep 2006, Graz, Austria.

Sloan, S.W., 2013. Geotechnical stability analysis. Géotechnique 63 (7), 531–571.

Sloan, S.W., Assadi, A., 1994. Undrained stability of a plane strain heading. Can. Geotech. J. 31 (3), 443–450.

Subrin, D., Wong, H., 2002. Tunnel face stability in frictional material: A New 3D failure mechanism. Comptes Rendus Mecanique 330 (7), 513–519.

Tschuchnigg, F., Schweiger, H.F., Sloan, S.W., 2015a. Slope stability analysis by means of finite element limit analysis and finite element strength reduction techniques. Part I: Numerical studies considering non-associated plasticity. Comput. Geotech. 70, 169–177.

Tschuchnigg, F., Schweiger, H.F., Sloan, S.W., Lyamin, A.V., Raissakis, I., 2015b. Comparison of finite-element limit analysis and strength reduction techniques. Géotechnique 65 (4), 249–257.

Yang, X.L., Huang, F., 2013. Three-dimensional failure mechanism of a rectangular cavity in a Hoek-Brown rock medium. Int. J. Rock Mech. Min. Sci. 61 (1), 189–195.

Yang, F., Zhao, L.H., Zhang, J., Yang, J.S., 2014. Investigation of finite element upper bound solution based on rigid translatory moving element. Rock and Soil Mechanics 35 (6), 1782–1786. In Chinese.

Yang, F., Zhang, J., Yang, J.S., Zhao, L.H., Zheng, X.C., 2015a. Stability analysis of unlined elliptical tunnel using finite element upper-bound method with rigid translatory moving elements. Tunn. Undergr. Space Technol. 50, 13–22.

Yang, F., Zhang, J., Zhao, L.H., Yang, J.S., 2016. Upper-bound finite element analysis of stability of tunnel face subjected to surcharge loading in cohesive-frictional soil. KSCE J. Civ. Eng. 20 (6), 2270–2279.

Yang, F., Sun, X.L., Zheng, X.C., Yang, J.S., 2017. Stability analysis of a deep buried elliptical tunnel in cohesive-frictional (c-ϕ) soils with a nonassociated flow rule. Can. Geotech. J. 54 (5), 736–741.

Yang, J.S., Zhang, J., Yang, F., 2015b. Stability analysis of shallow tunnel face using two-dimensional finite element upper bound solution with mesh adaptation. Rock Soil Mech. 36 (1), 257–264. In Chinese.

Zhang, F., Gao, Y.F., Wu, Y.X., Zhang, N., 2017. Upper-bound solutions for face stability of circular tunnels in undrained clays. Géotechnique 68 (1), 76–85.

Zheng, X., Pisanò, F., Vardon, P.J., Hicks, M.A., 2021. An explicit stabilised material point method for coupled hydromechanical problems in two-phase porous media. Comput. Geotech. 135, 104112.

Zheng, X., Pisanò, F., Vardon, P.J., Hicks, M.A., 2022. Fully implicit, stabilised MPM simulation of large-deformation problems in two-phase elastoplastic geomaterials. Comput. Geotech. 147, 104771.

Zou, J.F., Chen, G.H., Qian, Z.H., 2019. Tunnel face stability in cohesion-frictional soils considering the soil arching effect by improved failure models. Comput. Geotech. 106, 1–17.